NASA TECHNICAL NOTE

NASA TN D-8215

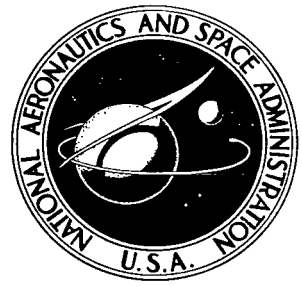

10° OFF-AXIS TENSILE TEST FOR INTRALAMINAR SHEAR CHARACTERIZATION OF FIBER COMPOSITES

Christos C. Chamis and John H. Sinclair

Lewis Research Center
Cleveland, Ohio 44135

NATIONAL AERONAUTICS AND SPACE ADMINISTRATION • WASHINGTON, D. C. • APRIL 1976

COMPLTD. 6/23/77 DM

ERRATA

NASA Technical Note D-8215

10^{o} OFF-AXIS TENSILE TEST FOR INTRALAMINAR SHEAR CHARACTERIZATION OF FIBER COMPOSITES

Christos C. Chamis and John H. Sinclair
April 1976

Page 9: The denominator of the second equation of equations (12) should be 3 instead of 2; that is, the equation should read

$$\epsilon_{cyy} = \frac{2\epsilon_{g2} + 2\epsilon_{g3} - \epsilon_{g1}}{3}$$

Page 9: Equation (13) should read

$$\epsilon_{\ell 12} = -0.456\,\epsilon_{g1} - 0.857\,\epsilon_{g2} + 1.313\,\epsilon_{g3} \qquad (13)$$

Issued March 1977

1. Report No.	2. Government Accession No.	3. Recipient's
NASA TN D-8215		

4. Title and Subtitle

10° OFF-AXIS TENSILE TEST FOR INTRALAMINAR SHEAR CHARACTERIZATION OF FIBER COMPOSITES

5. Report Date: April 1976

6. Performing Organization Code:

7. Author(s)

Christos C. Chamis and John H. Sinclair

8. Performing Organization Report No.: E-8577

9. Performing Organization Name and Address

Lewis Research Center
National Aeronautics and Space Administration
Cleveland, Ohio 44135

10. Work Unit No.: 506-17

11. Contract or Grant No.:

12. Sponsoring Agency Name and Address

National Aeronautics and Space Administration
Washington, D.C. 20546

13. Type of Report and Period Covered: Technical Note

14. Sponsoring Agency Code:

15. Supplementary Notes

16. Abstract

A combined theoretical and experimental investigation was conducted to assess the suitability of the 10° off-axis tensile test specimen for the intralaminar shear characterization of unidirectional composites. Composite mechanics, a combined-stress failure criterion, and a finite element analysis were used to determine theoretically the stress-strain variation across the specimen width and the relative stress and strain magnitudes at the 10° plane. Strain gages were used to measure the strain variation across the specimen width at specimen midlength and near the end tabs. Specimens from Mod-I/epoxy, T-300/epoxy, and S-glass/epoxy were used in the experimental program. It was found that the 10° off-axis tensile test specimen is suitable for intralaminar shear characterization and it is recommended that it should be considered as a possible standard test specimen for such a characterization.

17. Key Words (Suggested by Author(s))

Fiber composites; Intralaminar; Shear; Characterization; Theory; Experiment; Finite element; Standard test specimen; 10° off-axis; Tensile test

18. Distribution Statement

Unclassified - unlimited
STAR Category 24 (rev.)

19. Security Classif. (of this report)	20. Security Classif. (of this page)	21. No. of Pages	22. Price*
Unclassified	Unclassified	31	$4.00

* For sale by the National Technical Information Service, Springfield, Virginia 22161

CONTENTS

10^{o} OFF-AXIS TENSILE TEST FOR INTRALAMINAR SHEAR CHARACTERIZATION OF FIBER COMPOSITES

by Christos C. Chamis and John H. Sinclair

Lewis Research Center

SUMMARY

A combined theoretical and experimental investigation was conducted to assess the suitability of the 10^{o} off-axis tensile test specimen for the intralaminar shear characterization of unidirectional fiber composites. The theoretical part consisted of using composite mechanics, a combined stress failure criterion, and a finite element analysis to evaluate: the relative magnitudes of the stresses, strains, and shear modulus at the 10^{o} plane, the sensitivity of the stresses and strains to small errors in angle about 10^{o}, the angle between fiber and load directions at which the peak intralaminar shear strain occurs, the strain variation across the specimen width, and the influence of various degrees of restraint at the specimen end tabs.

The experimental part consisted of preparing, instrumenting, and testing specimens from Mod-I/epoxy, T-300/epoxy, and S-glass/epoxy fiber composites. These were selected to assess the applicability of the test specimen at high, intermediate, and low orthotropicity $E_{\ell 11}/E_{\ell 22}$ ratios, respectively. Delta rosette strain gages were used at the midlength and near the end tabs of the specimen to measure the strain variations across the specimen width at these locations. The test data obtained were reduced using a strain gage data reduction computer program and the results were plotted appropriately to generate the shear stress-strain curves to fracture for the three composite systems. Results obtained from this test method were compared with those obtained by other methods.

It was found that the 10^{o} off-axis tensile test specimen is suitable for intralaminar shear characterization and it is recommended that it should be considered as a possible standard test specimen for such a characterization.

INTRODUCTION

Efficient intralaminar (in-plane) shear characterization of unidirectional fiber composites has been a problem because of the difficulty of producing a state of pure shear in practical laboratory test specimens. For example, the simplest test specimen in use today is the three-point-bend short-beam-shear test specimen (ASTM D-2344-72). But this test specimen, while expedient for material quality control, is not suitable for generating design data because (1) this test produces nonuniform shear stress through the specimen's thickness and (2) the test yields only the fracture stress and not the total shear-stress shear-strain record to fracture. The most desirable test specimen is the thin tube subjected to torsion. This specimen provides pure shear stress and strain in the wall of the tube; however, the tube specimen is too expensive and time consuming to be practical and efficient. Between these two extremes, several other test specimens and procedures have been proposed for intralaminar shear characterization of unidirectional fiber composites (ref. 1). None of the available test specimens is completely satisfactory and researchers in the field are continuously looking for and proposing new ones.

One recent test specimen is the 10° off-axis tensile specimen proposed by IIT Research Institute during the course of an investigation under contract to NASA Lewis Research Center (ref. 2). This test specimen has several desirable features to qualify it as an efficient and a possible standard test for intralaminar shear characterization. However, it was recognized that before considering it as a possible standard, additional investigation was required from both the theoretical and experimental viewpoints.

Therefore, the objectives of the investigation reported herein were to perform both detailed theoretical and experimental studies in order to assess the suitability of the 10° off-axis tensile specimen for intralaminar shear characterization and the possibility for recommending it as a standard test specimen for such a characterization.

SYMBOLS

E normal modulus; subscripts define direction

F combined-stress failure criterion function

G shear modulus-intralaminar

K coupling coefficient in combined-stress failure criterion function

R strain transformation matrix

S uniaxial fracture stress; subscripts define direction

x, y, z	structural-axes orthogonal coordinate system with x taken along load direction
1, 2, 3	material-axes orthogonal coordinate system with 1 taken along fiber direction
ϵ	strain; subscripts define type, plane, and direction
θ	orientation angle between structural and material axes measured positive counterclockwise
θ_g	orientation angle locating strain gage from load direction
σ	stress; subscripts define type, plane, and direction
{ }	vector
[ ], [ ]$^{-1}$	square matrix, inverse

Subscripts:

C	compression
c	structural axes property
g	strain gage reading
ℓ	ply (unidirectional composite) property
S	shear, symmetric
T	tension
x, y, z	structural axes directions
1, 2, 3	material axes directions

THEORETICAL INVESTIGATION

The theoretical background leading to the investigation of the 10° off-axis tensile specimen for intralaminar shear characterization is discussed in this section. Specifically, the following are described: relative stress magnitudes at the 10° plane as assessed from force equilibrium and a combined-stress strength criterion; shear stress, shear strain, and shear modulus variation with orientation angle and their sensitivity at 10°; governing equations for predicting the intralaminar shear stress-strain curve; and finite element analysis of the stress variation across the width at the specimen midlength.

Relative Stress Magnitudes at the 10° Plane

A biaxial stress state is present when a 10° off-axis specimen is subjected to a uniaxial load. As is indicated in figure 1, this biaxial stress state consists of three stresses, longitudinal $\sigma_{\ell 11}$, transverse $\sigma_{\ell 22}$, and intralaminar shear $\sigma_{\ell 12}$ at the 10° plane. If a 10° off-axis specimen is to serve as a means for intralaminar shear characterization of a uniaxial composite, the intralaminar shear stress $\sigma_{\ell 12}$ must be the only one of these three stresses that is near its critical value, and fracture must occur at the 10° plane when $\sigma_{\ell 12}$ reaches this critical value. In the following section, it is shown through analysis of the stresses in the 10° off-axis specimen that this is the case. The relative magnitudes of the stresses involved are compared by using force equilibrium (or stress transformation) and a combined-stress failure criterion.

Relative stress magnitudes from force equilibrium. - The stresses in a ply with fibers oriented at an angle θ from the load direction as a function of the applied stress σ_{cxx} are given by the following well-known transformation equations which are easily derivable from force equilibrium considerations:

$$\sigma_{\ell 11} = \sigma_{cxx} \cos^2 \theta \tag{1}$$

$$\sigma_{\ell 22} = \sigma_{cxx} \sin^2 \theta \tag{2}$$

$$\sigma_{\ell 12} = \frac{1}{2} \sigma_{cxx} \sin 2\theta \tag{3}$$

The notation in equations (1) to (3) is as follows: σ denotes stress; θ is the orientation angle between applied stress (load direction) and the fiber direction; the subscripts c and ℓ denote composite and ply, respectively; the numerical subscripts 1 and 2 refer to an orthogonal right-hand coordinate system with 1 taken along the fiber direction. For the 10° off-axis specimen, substituting 10° for θ in equations (1) to (3) yields the following to three decimal figures:

$$\sigma_{\ell 11} = 0.970 \, \sigma_{cxx} \tag{4}$$

$$\sigma_{\ell 22} = 0.030 \, \sigma_{cxx} \tag{5}$$

$$\sigma_{\ell 12} = 0.171 \, \sigma_{cxx} \tag{6}$$

Equations (5) and (6) are used to assess the relative magnitudes of the transverse and

intralaminar shear stresses. As can be seen from equations (5) and (6), the intralaminar shear stress is about six times greater than the transverse stress.

Data comparing the relative magnitudes of the fracture strengths for a high modulus graphite epoxy system are presented in table I. In table I(a), under "Load direction", four types of specimens are listed. The first, second, and fourth were tensile specimens prepared from an eight-ply, flat, uniaxial $[0]_8$ laminate of Mod-I/epoxy (ERLA 4617). The specimens were cut out of the laminate so that the tensile axis of the 0° specimen was parallel to the fiber direction of the laminate, that of the 90° specimen was perpendicular to the fiber direction, and the tensile axis of the 10° specimen was offset 10° from the fiber direction of the laminate. The third specimen shown in table I(a) was a 5.08-centimeter- (2-in.-) diameter eight-ply Mod-I/epoxy tube with the graphite fibers running lengthwise along the tube. This tube was tested in torsion.

The fracture strength σ_{cxx} of the 10° off-axis composite (item 4, table I(a)) was 34.3×10^3 N/cm^2 (49.8 ksi). The corresponding fracture stresses of the plys at the 10° plane ($\sigma_{\ell 11}$, $\sigma_{\ell 22}$, and $\sigma_{\ell 12}$) as computed using equations (4) to (6) are presented in table I(b). The ratios of the computed ply fracture stresses to the measured uniaxial fracture strengths are shown in table I(c). As can be seen in table I(c), only the computed intralaminar shear stress is near its critical value. In fact, it is 12 percent greater than the measured corresponding strength $S_{\ell 12S}$. The computed longitudinal and transverse stresses are only 59 percent and 38 percent of their respective fracture stresses.

The important observation from the previous discussion is that when the 10° off-axis tensile specimen fails, only the intralaminar shear stress is near its critical value. This, therefore, leads to the conclusion that the 10° off-axis tensile specimen is suitable for measuring intralaminar shear strength of unidirectional fiber composites.

Relative stress magnitudes from combined-stress failure criteria. - In the previous section the relative stress magnitudes were compared on an individual stress basis and combined-stress interaction is not taken into account. To account for the interaction, a combined-stress failure criterion is required. The combined-stress failure criterion used herein is derivable from a modified distorion energy principle and is described in references 3 and 4. When both the ply longitudinal and the transverse stresses are tensile, as is the case for the 10° off-axis tensile specimen, the failure criterion to determine whether fracture has occurred is

$$1 - \left[\left(\frac{\sigma_{\ell 11}}{S_{\ell 11T}}\right)^2 + \left(\frac{\sigma_{\ell 22}}{S_{\ell 22T}}\right)^2 - K_{\ell 12}\,\frac{\sigma_{\ell 11}\sigma_{\ell 22}}{S_{\ell 11T}S_{\ell 22T}} + \left(\frac{\sigma_{\ell 12}}{S_{\ell 12S}}\right)^2\right] \leq 0 \qquad (7)$$

where S denotes uniaxial fracture stress, K is a coupling coefficient which depends on the elastic constants of the composite material (ref. 3 or 4), the subscript T denotes tension and S denotes shear. Using numerical values for σ and S from table I(a) and the corresponding K value of 1.44 as determined in references 3 and 4, the left side of equation (7) yields

$$1 - \left[\left(\frac{48.3}{81.7}\right)^2 + \left(\frac{1.5}{4.0}\right)^2 - 1.44\,\frac{48.3\times1.5}{81.7\times4.0} + \left(\frac{8.5}{7.6}\right)^2\right]$$

which reduces to

$$1 - [0.350 + 0.141 - 0.319 + 1.25] = -0.421$$

Since this value is less than zero, according to the failure criterion, fracture has occurred. The important observation to be noted here is that the major stress contribution to fracture is from the intralaminar shear stress which is the last term in the brackets. The contribution from the longitudinal and transverse stresses (first three terms in the brackets) tend to cancel each other. It is worth noting that the cancellation tendency observed here is not exhibited when the relative magnitudes are compared on an individual stress basis.

The numerical results from the combined-stress failure criterion just discussed lead to the conclusion that fracture of the 10° off-axis tensile specimen is initiated by the intralaminar shear stress.

Sensitivity of Material-Axes Stresses and Strains With Errors in Orientation Angle

An assessment of how sensitive the material-axes stresses and strains are with small errors in the load orientation angle may be obtained by plotting these stresses against orientation angle. This is illustrated in figure 2, where the ply stresses plotted have been normalized with respect to composite stress along the load direction. The important point to be observed from this figure is that in the region of a load angle of 10°, the transverse and intralaminar shear stresses vary more rapidly than the longitudinal stress on a relative basis. It can be shown that a 1° change (e.g., $\theta = 11^{\circ}$ in eqs. (1) to (3)) in load angle produces a change of about 21 percent in the transverse

stress, a 10-percent change in the intralaminar shear stress, and only a 0.6-percent change in the longitudinal stress.

The variation of the material-axes strains as a function of load angle is plotted in figure 3 for a Mod-I/epoxy unidirectional composite. As can be observed in this figure, the material-axes shear strain (intralaminar shear strain $\epsilon_{\ell 12}$) is maximum at about a 10° load orientation angle and appears to be insensitive to small errors about this angle. These are significant results because they are desirable features for the test specimen proposed to measure the intralaminar shear modulus and fracture shear stress. Though results are not presented here, the two other composites investigated approach their peaks at about 11° for T-300/epoxy (PR288) and 15° for S-glass/epoxy (PR288).

The variation of the structural-axes shear modulus G_{cxy} as a function of load angle is also of interest. This is illustrated in figure 4. Note that, when the load angle θ is 10°, G_{cxy} changes rather slowly. For example, a 1° change in θ produces about 0.3 percent change in G_{cxy}.

It is interesting to note that the 45° off-axis tensile specimen has been used to measure ply intralaminar shear properties and to generate data for stress-strain curves. The motivation for its usage is the plateau of both ply intralaminar shear stress $\sigma_{\ell 12}$ and composite modulus G_{cxy} at $\theta = 45^{\circ}$ (figs. 2 and 4). The major drawback with the 45° off-axis tensile specimen is that both ply intralaminar shear and transverse stresses have the same magnitudes (fig. 2) at $\theta = 45^{\circ}$. Therefore, the following will occur:

(1) The shear stress-strain curve will reflect considerable ply transverse tensile behavior.

(2) Specimen fracture will be caused by transverse tension since the transverse fracture stress $S_{\ell 22T}$ is about one-half of the intralaminar shear fracture stress $S_{\ell 12S}$ (table I(a)).

The previous discussion leads to the following conclusion. Since ply intralaminar shear stress of the 10° off-axis tensile specimen is sensitive to small misorientation errors, care should be taken in fiber orientation, strain gage positioning, and load alinement. It is recommended that these be kept within $\pm 1^{\circ}$. However, if the fracture intralaminar shear strain is sought, then the misorientation is not as critical since the intralaminar shear strain peaks at load angle of about 10° and is insensitive to small errors about this angle.

Equations for Generating the Ply Intralaminar Shear Stress-Strain Curve

The sets of equations required to generate the ply intralaminar shear stress-strain curves are described in this section. The matrix equation relating structural axes

strains to strain gage actual strains (refer to figs. 1 and 5) is

$$\begin{Bmatrix} \epsilon_{g1} \\ \epsilon_{g2} \\ \epsilon_{g3} \end{Bmatrix} = \begin{bmatrix} \cos^2 \theta_{g1} & \sin^2 \theta_{g1} & \frac{1}{2} \sin 2\theta_{g1} \\ \cos^2 \theta_{g2} & \sin^2 \theta_{g2} & \frac{1}{2} \sin 2\theta_{g2} \\ \cos^2 \theta_{g3} & \sin^2 \theta_{g3} & \frac{1}{2} \sin 2\theta_{g3} \end{bmatrix} \begin{Bmatrix} \epsilon_{cxx} \\ \epsilon_{cyy} \\ \epsilon_{cxy} \end{Bmatrix} \tag{8}$$

or in compact form

$$\{\epsilon_g\} = [R] \{\epsilon_c\} \tag{9}$$

The notation in equation (8) is as follows: ϵ_{g1}, ϵ_{g2}, and ϵ_{g3} denote the true strain from gages 1, 2, and 3, respectively (fig. 5); θ_{g1}, θ_{g2}, and θ_{g3} denote the corresponding orientation angles measured from the load direction; ϵ_{cxx}, ϵ_{cyy}, and ϵ_{cxy} denote the structural axes strains. It is important to note that the true strains are determined taking into account gage transverse sensitivity provided by the strain gage manufacturer (ref. 5).

The equation relating the ply intralaminar shear strain to structural-axes strain for any θ orientation is

$$\epsilon_{\ell 12} = (\epsilon_{cyy} - \epsilon_{cxx}) \sin 2\theta + \epsilon_{cxy} \cos 2\theta \tag{10}$$

The structural axes strains $\{\epsilon_c\}$ are obtained from equation (9) as follows:

$$\{\epsilon_c\} = [R]^{-1} \{\epsilon_g\} \tag{11}$$

where $[R]^{-1}$ denotes the inverse of $[R]$. In expanded form, equation (11) for a 60°-delta rosette ($\theta_{g1} = 0^\circ$; $\theta_{g2} = 120^\circ$; $\theta_{g3} = 240^\circ$) is

$$\left.\begin{aligned} \epsilon_{cxx} &= \epsilon_{g1} \\ \epsilon_{cyy} &= \frac{2\epsilon_{g2} + 2\epsilon_{g3} - \epsilon_{g1}}{3} \\ \epsilon_{cxy} &= \frac{2(\epsilon_{g3} - \epsilon_{g2})}{\sqrt{3}} \end{aligned}\right\} \tag{12}$$

The intralaminar shear strain along the 10^{o} plane is obtained by substituting the structural-axis strains from equation (12) in equation (10) and setting $\theta = 10^{o}$. The resulting equation in three decimal figures is

$$\epsilon_{\ell 12} = -0.456\,\epsilon_{g1} - 0.857\,\epsilon_{g2} + 1.313\,\epsilon_{g3} \tag{13}$$

The expanded form of equation (11) for a rectangular rosette ($\theta_{g1} = 0^{o}$; $\theta_{g2} = 45^{o}$; and $\theta_{g3} = 90^{o}$) is

$$\left.\begin{aligned} \epsilon_{cxx} &= \epsilon_{g1} \\ \epsilon_{cyy} &= \epsilon_{g3} \\ \epsilon_{cxy} &= -\epsilon_{g1} + 2\epsilon_{g2} - \epsilon_{g3} \end{aligned}\right\} \tag{14}$$

The intralaminar shear strain along the 10^{o} plane is obtained in the same way as described for the 60^{o}-delta rosette. The resulting equation is

$$\epsilon_{\ell 12} = -1.282\,\epsilon_{g1} + 1.879\,\epsilon_{g2} - 0.598\,\epsilon_{g3} \tag{15}$$

As can be seen from equations (13) and (15) the calculation for the intralaminar shear strain is simple once the true gage strains are known. As was already mentioned, ϵ_{g1}, ϵ_{g2}, and ϵ_{g3} are the true gage strains in that they account for gage transverse sensitivity.

The equation relating the ply intralaminar shear stress to the structural-axes stress in equation (6) which was described previously is repeated here for convenience

$$\sigma_{\ell 12} = 0.171\ \sigma_{cxx} \tag{6}$$

The procedure for generating the intralaminar shear stress-strain curve is as follows: For each load increment,

(1) Calculate the intralaminar shear strain from either equation (13) for a 60^{o}-delta rosette or from equation (15) for a rectangular rosette.

(2) Calculate the ply intralaminar shear stress $\sigma_{\ell 12}$ from equation (6).

(3) Plot $\sigma_{\ell 12}$ calculated in item (2) against $\epsilon_{\ell 12}$ calculated in item (1).

The initial ply shear modulus is determined from the slope of the initial tangent to the stress-strain curve plotted in item (3). The shear modulus at any other point may be determined from the slope of the tangent to the curve at that point. The ply intralaminar shear strength equals the shear stress calculated in item (2) at the fracture load. The ply intralaminar fracture strain is the shear strain calculated at the fracture load in item (1).

It is important to note that the generation of the intralaminar shear stress-strain curve from the procedure just described requires the simultaneous readings of <u>three</u> strain gages and the relatively simple calculations already indicated.

Axial Stress Variation Across the Specimen Width at Midlength Via Finite Element Analysis

The 10^{o} off-axis tensile specimen will tend to undergo in-plane bending. This is caused by the coupling between normal and shear deformations: this coupling will tend to deform the specimen in shear. However, the grips prevent the specimen ends from shearing thereby inducing in-plane bending. This in-plane bending induces an axial stress variation across the specimen width.

In order to obtain a theoretical assessment of the axial stress variation due to in-plane bending, a finite element analysis was performed. The element used is a second-order triangular plate finite element with six nodes and two displacement degrees of freedom (DOF) per node. A schematic of the finite element representation is shown in figure 6. The dimensions shown in the schematic are those of the actual test specimen used. Note the finite element representation includes the tapered end-tab portions projecting beyond the grip ends. Note also that the finite element representation consists of 288 elements, 657 nodes, and 1314 DOF.

The analysis was performed on a specimen made from Mod-I/epoxy and having three different boundary conditions. The boundaries were selected to simulate the following:

(1) Fixed ends, induces in-plane bending

(2) Pinned ends, free from in-plane bending

(3) End load equivalent to produce an end restraint intermediate to (1) and (2).

The finite element analysis results are presented graphically in figure 7. The actual boundary conditions of the specimen produce a stress variation somewhere between (1) and (2) and probably close to (3). The important points to be observed from the curves in figure 7 are:

(1) At the specimen center all boundary conditions induce approximately the same axial stress which is equal to the average stress P/A in the specimen.

(2) The axial stress variation across the specimen width will be less than 10 percent assuming the dash-dotted curve is the best approximation.

(3) The axial stress at one edge may be 2 to 5 percent higher than the axial stress at the center. This observation has the following significant implication. Because the edge stress is higher, fracture will probably initiate at the edge. The average axial stress as predicted by P/A will be a few percent less than the axial stress at the edge which initiates fracture. Therefore, the intralaminar fracture stress predicted by equation (6) is on the conservative side. Although no results are presented herein, varying the end tab material had negligible effect on the axial stress variation across the width at the specimen midlength.

The previous discussion leads to the following important conclusions:

(1) Ply intralaminar shear stresses calculated from equation (6) using the average axial stress are accurate to within 5 percent.

(2) Ply intralaminar fracture stress (ply intralaminar shear strength) determined from a 10° off-axis tensile specimen will tend to be a few percent below the actual value and, therefore, on the conservative side.

EXPERIMENTAL INVESTIGATION

The experimental program performed to assess the suitability of 10° off-axis tensile specimens for intralaminar shear characterization is covered in this section.

Composite Systems

The composite systems used in this investigation consisted of Mod-I/epoxy, T-300/epoxy, and S-glass/epoxy. These were selected in order to determine the applicability of the test specimen at high, intermediate, and low orthotropicity (longitudinal modulus to transverse modulus $E_{\ell 11}/E_{\ell 22}$) ratios, respectively.

Laminate Fabrication

The laminate consisting of eight unidirectional plies of Mod-I graphite fibers in a matrix of ERLA 4617 epoxy resin cured with MPDA was fabricated by a commercial vendor. The vendor used the following curing procedure. The laminate was heated from room temperature to 121° C (250° F) under a partial vacuum of approximately 2 N/cm^2 (3 psi) and held for 40 minutes at this temperature. It was then heated to 177° C (350° F) under an autoclave pressure of 34.5 N/cm^2 (50 psi) and held for 2 hours. Pressure was maintained until it had cooled to 40° C (120° F).

The other unidirectional, eight-ply laminates were prepared at the Lewis Research Center using commercially manufactured prepregs of fibers in PR288 epoxy resin. Prepreg laminates were built up in molds treated with a commercial release agent. The loaded molds were then placed in a press preheated to 149° C (300° F) and contact pressure was applied for 3.6 minutes. Pressure was then gradually increased to 207 N/cm^2 (300 psi) within a span of 2 minutes to allow escape of entrapped gases and to enhance uniform resin distribution. This pressure was maintained for 2 hours, at which time pressure was released and the laminates were removed immediately from the hot molds.

Unidirectional composite properties as determined experimentally at Lewis are presented in table II. These are single specimen data.

Specimen Preparation, Instrumentation, and Testing

A drafting machine was used to lay out tensile specimens at the desired load angles on the laminate plates. The specimens were then cut slightly overwidth by a 0.061-centimeter- (0.024-in.-) thick diamond wheel mounted on a surface grinder. Stacks of specimens, so cut, were placed on edge and dressed down to the required 1.27-centimeter (0.500-in.) width by a diamond wheel. Specimen ends were reinforced with adhesively bonded fiberglass tabs. It is noted that ASTM recommended standards were not followed in this procedure.

Tensile specimens were instrumented with either one or five strain gages, type EA-13-030YB-120, 60° delta rosette, arranged as shown in figure 8. The test specimens were placed in the grips pictured in figure 9 and loaded to fracture using a hydraulically actuated universal testing machine. Loading was incremental to facilitate periodic recording of strain gage data.

Experimental Results

The experimental results consist of stress-strain curves, axial strain variations across the tensile specimens, and determination of shear moduli from stress-strain data. Comparisons of these shear moduli are made with those obtained from thin tubes and for other fiber layups as well as some literature values.

Stress-Strain Curves

The strain gage data reduction computer program (SGDR) (ref. 6) was used to generate stress-strain curves from the incremental loads and corresponding data recorded from the strain gages. A sample of these data is shown in table III. The data for the Mod-I/epoxy specimen which had five strain gages arranged as shown in figure 8 are presented in figures 10 to 12. The figures show curves for the five gage positions superimposed on one plot for structural axes stresses σ_{cxx}, Poisson's strains ϵ_{cyy}, and shear strains ϵ_{cxy}, respectively, plotted as a function of axial strains ϵ_{cxx}.

As can be seen in figure 10, the magnitude of the strains at a given axial stress do not vary greatly from site to site. For example, at a stress of 2.1×10^4 N/cm^2 (30 ksi), the strain at the midlength center of the specimen (gage 2) is about 0.17 percent while the strains near the edges midlength (gages 1 and 3) are around 0.19 percent. Since the edges of the specimen at midlength appear to have elongated a little more than the center, it is possible that the specimen twisted somewhat out-of-plane during the tensile test.

Figure 11 shows Poisson's strains as a function of axial strains. At any level of axial strain ϵ_{cxx}, it can be seen that the Poisson's strains ϵ_{cyy} are larger at the specimen edges than at the center. Note that the difference is magnified because of the large scale on the ordinate. This is true both near the tabs and at the specimen midlength. The cause for this behavior is probably due to coupling between normal, shear strains, and transverse strain in the presence of the possible out-of-plane twisting mentioned previously.

The coupled shear-strains are shown in figure 12 as a function of the axial strains. They do not appear to vary much from gage site to gage site and may be within the limits of experimental error.

Axial Strain Variations Across Specimen Widths

Axial strains at fracture are shown in figures 13 and 14 for Mod-I/epoxy and

S-glass/epoxy unidirectional composite laminates loaded at 10^{o} from the fiber direction. These data taken directly from the stress-strain data are accompanied on the figures with schematics of the specimens and plots of strain against gage location.

For Mod-I (fig. 13), the experimentally measured fracture strains are slightly higher at the specimen edges than at the center (0.320 percent and 0.336 percent compared to 0.287 percent) for the gages located at the midlength. Near the tensile grips, however, the strain was higher halfway across the specimen (0.305 percent) than near the edge (0.288 percent). It is suspected that these differences are due primarily to the restraining effects of the grips. The important point to observe is that the difference between the axial strains at the edges (at the specimen midlength) is less than 5 percent.

Strain variations for S-glass/epoxy are shown in figure 14 for a tensile stress of 2.2×10^{4} N/cm^{2} (31.6 ksi) and at fracture 4.2×10^{4} N/cm^{2} (60.3 ksi). The main point to be noted here is that this material elongates much more than the Mod-I/epoxy (~1.3 percent against 0.3 percent). The edge strain difference at the midlength of the specimen at fracture is less than 1 percent and probably is within the experimental error band. Near the tabs, however, the strain measurements of 1.12 percent near the specimen edge and 1.54 percent midway across the specimen probably represent a real difference induced by end restraining.

Shear Stress-Strain Curves

Intralaminar shear stress-strain curves of the 10^{o} off-axis tensile specimen for Mod-I/epoxy, S-glass/epoxy, and T-300/epoxy are presented in figure 15. The intralaminar shear stresses and shear strains were calculated from data obtained from the SGDR program (table III) by using equations (6) and (10). Note equation (13) could also have been used. The intralaminar shear stresses $\sigma_{\ell 12}$ thus obtained were plotted against the intralaminar shear strains $\epsilon_{\ell 12}$ calculated for the corresponding longitudinal tensile stresses.

From the intralaminar shear stress-strain curves, the intralaminar shear moduli were determined as previously described. Three moduli were determined for each material, initial tangent, secant, and final tangent. These values are shown in table IV. The initial tangent was drawn on the intralaminar shear stress-strain diagram at a strain of 0.1 percent. The final tangent shear modulus is the slope of the shear-strain curve at the fracture load, and the secant shear modulus is the slope of the line connecting the origin with the fracture point on the stress-strain curve.

Observations of the intralaminar shear stress-strain diagrams (fig. 15), or the table IV values, reveal that initially the S-glass composite is most resistant to shear deformation followed by the Mod-I and T-300 in that order. At failure, however,

Mod-I is more resistant to shear with S-glass having the least shear resistance. Note the extensive nonlinearity of the diagrams for the S-glass and T-300 curves.

A photograph of the Mod-I fractured specimen is shown in figure 16. As can be seen in this figure, the fracture occurred at the gage section along the fiber direction indicating intralaminar shear fracture.

Comparisons of Mod-I/Epoxy Shear Stress-Strain Curves for Different Configurations and Layups

Shear stress-strain curves for some additional Mod-I/epoxy configurations along with the curve for $[0]_8$ tested at 10° from the fiber direction (10° off-axis tensile specimen) are shown in figure 17 for comparison purposes. The additional curves are for a $[0_2, 90_2]_S$ laminate tested at 10° to the 0° fiber direction, a $\pm 45^\circ$ laminate, and for a unidirectional thin tube tested in torsion in the Lewis Research Center Multiaxial Testing Facility (ref. 7). The shear moduli for these materials are tabulated in table V. Note that the initial tangent shear moduli are approximately the same for all four tests. However, as can be observed from figure 17, the fracture shear strains of the 10° off-axis tensile specimen and the thin tube are about the same. Those for the other two are about 30-percent lower. This lower value reflects the presence of transverse lamination residual stress in the $[0_2, 90_2]_S$ (tested at 10°) and the $[(\pm 45)_2]_S$ laminates.

The important observation from the previous discussion is that the 10° off-axis tensile specimen had an intralaminar fracture shear strain practically identical to that of the thin tube tested in torsion and a corresponding stress about 0.66×10^3 N/cm^2 (1 ksi) higher. Therefore, the 10° off-axis tensile specimen should be suitable for intralaminar shear characterization.

COMPARISONS

The measured and finite element predicted structural axes shear strains are plotted in figure 18 for the same axial stress for comparison purposes. As can be seen, the comparison is reasonable. It is noted that this comparison was selected because of the predominance of the structural axes shear strains relative to the other two strains (figs. 10 to 12) in equations (10) or (13).

The measured-initial-tangent intralaminar shear moduli and fracture stresses are compared with those available elsewhere (low and high values) in table VI. As can be

seen, the measured data from the 10^{o} off-axis tensile specimen are within the range of the values reported elsewhere. The spread in the available data is due to variations in fiber volume ratio (0.45 to 0.70) and due to the test method used.

The previous comparisons lead to the conclusion that the 10^{o} off-axis tensile specimen appears to be a good specimen for intralaminar shear characterization from both the theoretical and experimental viewpoints.

RECOMMENDATION

Based on the theoretical and experimental results of this investigation, it is recommended that the 10^{o} off-axis tensile test specimen be considered as a possible standard test specimen for characterizing the intralaminar shear properties of unidirectional fiber composites.

A schematic depicting the geometry and instrumentation of the recommended standard test specimen is shown in figure 19. Note that it is advisable to use two back-to-back delta rosette strain gages to account for possible out-of-plane bending. The procedures previously described may be used for specimen preparation, instrumentation, mounting in the test fixture, and data acquisition and reduction. The ASTM D3039-74 test procedure may also be used as a guide.

The distinct advantages of the 10^{o} off-axis tensile specimen as a standard for intralaminar shear characterization compared to current practice are:

(1) Use of a familiar tensile test procedure (ASTM D3039-74)

(2) Use of thin laminate narrow specimens which save considerable material compared to thin tubes

(3) Test specimens may be cut from the same laminate as test specimens for longitudinal and transverse properties characterization

(4) Specimens have uniform shear stress through the thickness

(5) Specimens can be easily adapted to testing for environmental and elevated temperature effects

(6) Specimens can be readily used for fatigue testing

(7) Specimens are suitable for dynamic and impact loading characterization

(8) The test yields, in addition to intralaminar shear properties, the following off-axis properties: modulus, Poisson's ratio, coupling between extensional and shear deformations, and fracture stress

(9) Specimens are free of lamination residual stresses in contrast to the $\pm 45^{o}$ specimen

(10) The intralaminar shear strain reaches or approaches its maximum when the angle between load and fiber directions is about 10^{o}

The disadvantages of the suggested standard test specimen are:

(1) Need to measure three strains at a point

(2) Need to transform both strains and stresses

(3) Care in test specimen preparation

(4) Care in alining strain gage on specimen and specimen in load fixture

CONCLUSION

A combined theoretical and experimental investigation was performed to assess the applicability of the 10° off-axis tensile specimen for the intralaminar shear characterization of unidirectional fiber composites. The results of this investigation led to the recommendation that the 10° off-axis tensile specimen be considered as a possible standard test for intralaminar shear characterization of unidirectional fiber composites.

Lewis Research Center,
National Aeronautics and Space Administration,
Cleveland, Ohio, February 12, 1976,
506-17.

REFERENCES

1. Bert, C. W.: Experimental Characterization of Composites. Composite Materials, Vol. 8, Pt. 2, C. C. Chamis, ed., Academic Press, 1975, pp. 73-133.

2. Daniel, I. M.; and Liber, T.: Lamination Residual Stresses in Fiber Composites. (IITRI-D6073-1, IIT Research Inst.; NAS3-16766) NASA CR-134826, 1975.

3. Chamis, Cristos C.: Failure Criteria for Filamentary Composites. NASA TN D-5367, 1969.

4. Chamis, C. C.: Failure Criteria for Filamentary Composites. STP 460, Composite Materials: Testing and Design, Am. Soc. for Testing and Materials, 1972, pp. 336-351.

5. Transverse Sensitivity Errors. TN-137, Micro-Measurements.

6. Chamis, C. C.; Kring, J. F.; and Sullivan, T. L.: Automated Testing Data Reduction Computer Program. NASA TM X-68050, 1972.

7. Chamis, C. C.; and Sullivan, T. L.: Combined-Load Stress-Strain Relationships of Fiber Composite Laminates. NASA TM X-71825, 1976.

TABLE I. - FRACTURE STRESSES AND COMPARISON WITH PLY STRENGTHS FOR MOD-I/EPOXY SPECIMENS

(a) Measured ply strengths

Load direction	Strength	
	N/cm^2	ksi
0^o (longitudinal tensile $S_{\ell 11T}$)	56.3×10^3	81.7
90^o (transverse tensile $S_{\ell 22T}$)	2.8	4.0
0^o Tube (torsion $S_{\ell 12S}$)	5.2	7.6
10^o	34.3	49.8

(b) Computed ply fracture stresses at the 10^o plane

Stress type	Fracture stress	
	N/cm^2	ksi
Longitudinal $\sigma_{\ell 11}$ (along fibers)	33.3×10^3	48.3
Transverse to fibers $\sigma_{\ell 22}$	1.0	1.5
Intralaminar shear $\sigma_{\ell 12}$	5.9	8.5

(c) Comparison of ply fracture stresses at the 10^o plane ply strengths

Stress type	Ply strength		Computed ply fracture stress at the 10^o plane		Ratio of computed ply fracture stress to ply strength
	N/cm^2	ksi	N/cm^2	ksi	
Longitudinal	56.3×10^3	81.7	33.3×10^3	48.3	0.59
Transverse	2.8	4.0	1.0	1.5	.38
Intralaminar shear	5.2	7.6	5.9	8.5	1.12

TABLE II. - UNIDIRECTIONAL COMPOSITE PROPERTIES

Property	Composite		
	Mod-I/epoxy	T-300/epoxy	S-glass/epoxy
Longitudinal tensile modulus, $E_{\ell 11}$, N/cm^2 (psi)	24.1×10^6 (34.9×10^6)	13.2×10^6 (19.1×10^6)	4.72×10^6 (6.84×10^6)
Transverse tensile modulus, $E_{\ell 22}$, N/cm^2 (psi)	0.772×10^6 (1.12×10^6)	0.800×10^6 (1.16×10^6)	1.34×10^6 (1.94×10^6)
Shear modulus, $G_{\ell 12}$, N/cm^2 (psi)	0.610×10^6 (0.89×10^6)	0.434×10^6 (0.63×10^6)	0.648×10^6 (0.94×10^6)
Longitudinal Poisson's ratio, $\nu_{\ell 12}$	0.218	0.394	0.316
Longitudinal tensile fracture stress, $S_{\ell 11T}$, N/cm^2 (ksi)	56.3×10^3 (81.7)	128×10^3 (186)	129×10^3 (188)
Transverse tensile fracture stress, $S_{\ell 22T}$, N/cm^2 (ksi)	2.8×10^3 (4.0)	4.2×10^3 (6.2)	4.5×10^3 (6.5)

TABLE III. - COMPUTER OUTPUT FOR CENTER GAGE OF MOD-I/EPOXY SPECIMEN

(Refer to fig. 5 for strain gage orientation)

Axial load				Apparent strains, percent			Actual strains,[a] percent			Structural axis strains, percent		
kg	lb	Stress		Gage 1	Gage 2	Gage 3	Gage 1	Gage 2	Gage 3	ϵ_{cxx}	ϵ_{cyy}	ϵ_{cxy}
		N/cm^2	ksi									
11.3	25	0.62×10^3	0.90	0.01	~0	~0	0.01	~0	~0	~0	~0	-0.01
22.7	50	1.24	1.79	.02	~0	~0	.02	~0	~0	.01	~0	-.02
45.4	100	2.47	3.59	.04	-.01	~0	.04	-.01	~0	.02	~0	-.06
136	300	7.42	10.8	.12	-.04	-.01	.12	-.04	-.01	.06	-.01	-.18
227	500	12.4	17.9	.20	-.06	-.01	.21	-.07	-.02	.10	-.02	-.31
318	700	17.3	25.1	.29	-.09	-.02	.29	-.09	-.02	.14	-.02	-.45
408	900	22.2	32.3	.38	-.12	-.02	.38	-.13	-.03	.18	-.03	-.58
499	1100	27.2	39.4	.47	-.15	-.03	.47	-.16	-.04	.22	-.04	-.73
590	1300	32.1	46.6	.57	-.20	-.04	.58	-.20	-.04	.27	-.04	-.90
630	[b]1390	34.4	49.8	----	-----	-----	----	-----	-----	.29	-.05	-.99

[a]These are apparent strains corrected for transverse sensitivity.

[b]Fracture load = 630 kg (1390 lb) structural axis strains were extrapolated by computer program SGDR.

TABLE IV. - SHEAR MODULI FOR THREE LAMINATES AS DETERMINED EXPERIMENTALLY USING 10° OFF-AXIS TENSILE TEST

Laminate material	Initial tangent		Secant		Final tangent	
	Shear modulus					
	N/cm^2	psi	N/cm^2	psi	N/cm^2	psi
Mod-I/epoxy	0.61×10^6	0.88×10^6	0.57×10^6	0.83×10^6	0.47×10^6	0.68×10^6
T-300/epoxy	.43	.63	.24	.35	.12	.17
S-glass/epoxy	.65	.94	.20	.30	.08	.11

TABLE V. - SHEAR MODULI FOR SEVERAL CONFIGURATIONS OF Mod-I/EPOXY LAMINATES

Laminate configuration	Initial tangent		Secant		Final tangent	
	Shear modulus					
	N/cm^2	psi	N/cm^2	psi	N/cm^2	psi
$[0]_8$ tested at 10°	0.61×10^6	0.88×10^6	0.57×10^6	0.83×10^6	0.47×10^6	0.68×10^6
$[0_2, 90_2]_S$ tested at 10°	.60	.87	.56	.81	.54	.78
$[(\pm45)_2]_S$	.62	.90	.61	.88	.53	.76
Thin tube with fibers parallel to tube length tested in torsion	.59	.86	.48	.70	.31	.45

TABLE VI. - COMPARISON OF MEASURED INTRALAMINAR SHEAR PROPERTIES FROM 10° OFF-AXIS TENSILE SPECIMEN WITH THOSE REPORTED ELSEWHERE

Composite	10° Off-axis tensile specimen		Reported elsewhere				10° Off-axis tensile specimen		Reported elsewhere			
			Low		High				Low		High	
	Modulus						Fracture stress					
	N/cm^2	psi	N/cm^2	psi	N/cm^2	psi	N/cm^2	ksi	N/cm^2	ksi	N/cm^2	ksi
Mod-I/epoxy	0.61×10^6	0.88×10^6	0.44×10^6	0.64×10^6	0.62×10^6	0.90×10^6	5.9×10^3	8.6	4.7×10^3	6.8	6.1×10^3	8.9
T-300/epoxy	.43	.63	.42	.61	.69	1.00	8.3	12.1	6.2	9.0	9.2	13.3
S-glass/epoxy	.65	.94	.57	.83	1.2	1.74	7.1	10.3	4.5	6.5	12	17.1

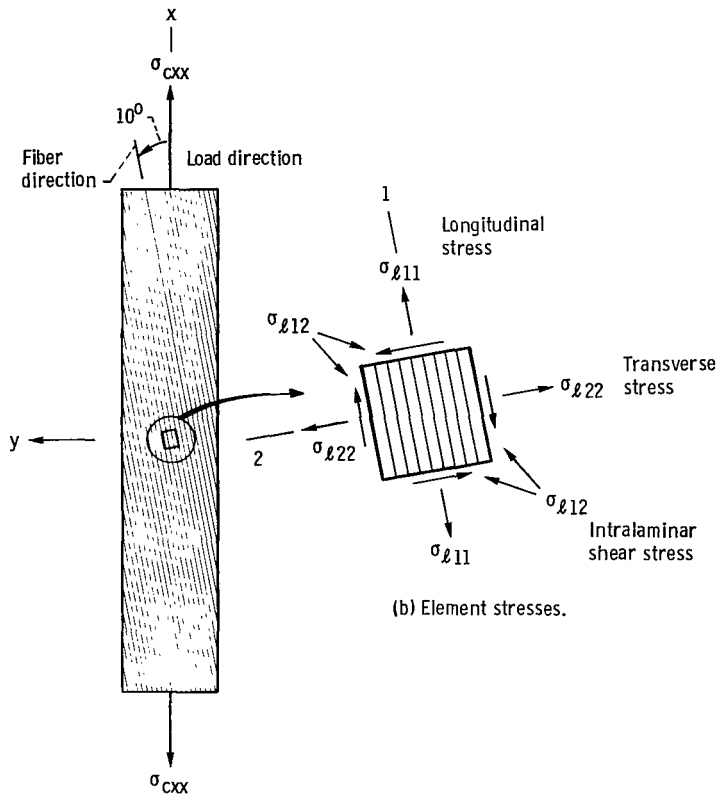

(a) Loaded specimen.

(b) Element stresses.

Figure 1. - Schematic depicting loaded 10^0 off-axis tensile test specimen and stresses at element at 10^0-plane (x, y - structural axes; 1, 2 - material axes).

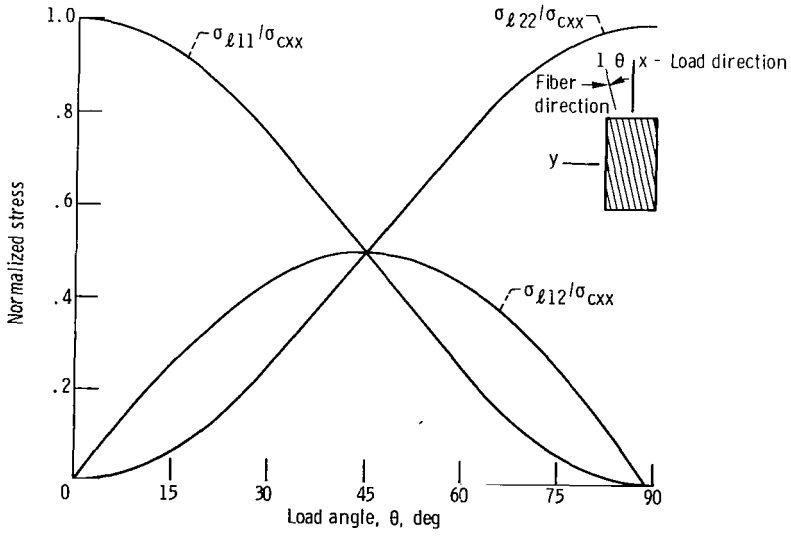

Figure 2. - Variation of material axes stress in unidirectional composite plotted against load direction.

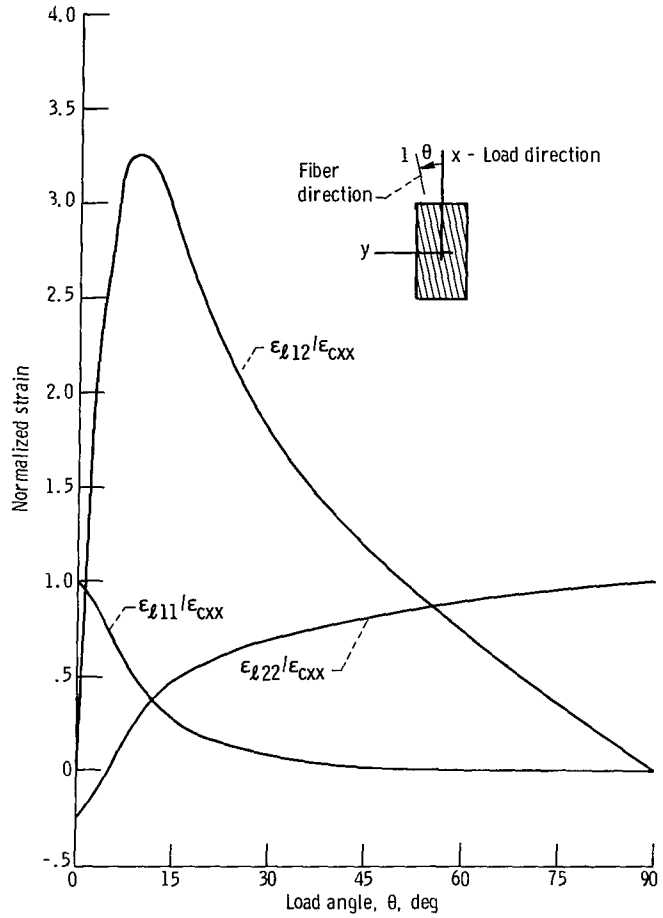

Figure 3. - Variation of material axes strains in unidirectional composite (Mod-I/epoxy) plotted against direction.

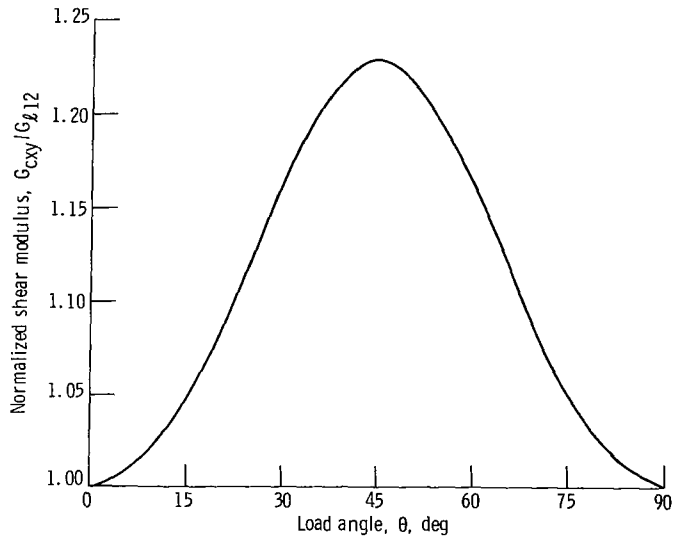

Figure 4. - Variation of shear modulus with load direction.

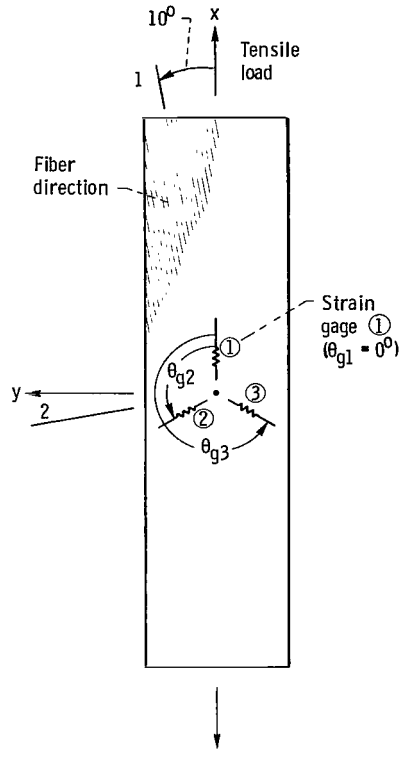

Figure 5. - Schematic depicting 10° off-axis tensile test specimen with strain gage positions (x, y - structural axes; 1, 2 - material axes).

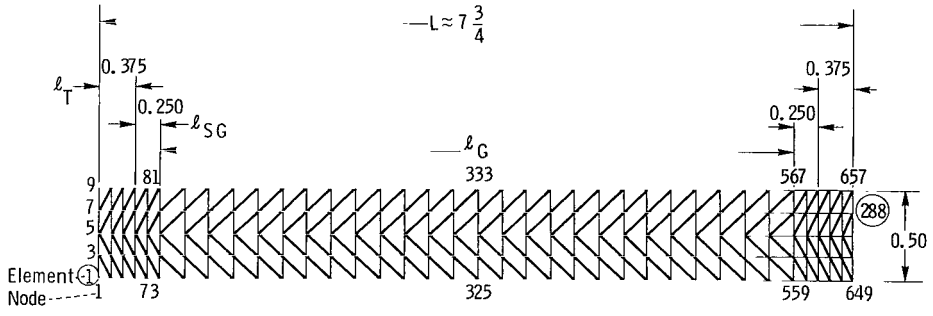

SYMBOLS:

L	length of test section ℓ_G plus tapered portion of end tabs
ℓ_T	length of tapered portion of Micarta end tabs
ℓ_{SG}	section just beyond tapered portion of end tabs and site of top gages

Figure 6. - Grid for finite element analysis of Mod-I/epoxy specimens. (Top gages located at nodes 74 and 77; midpoint gages located at nodes 326, 329, and 332. All dimensions shown are relative.)

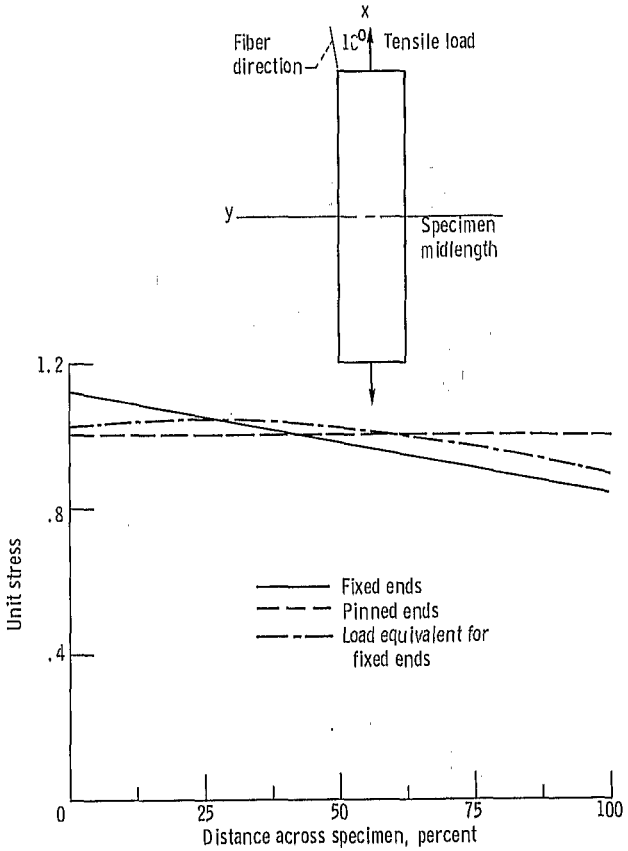

Figure 7. - Finite element analysis results of axial stress variation at midlength for three different boundary conditions; Mod-I/epoxy 10^0 off-axis tensile specimen. (See fig. 6 for finite element representation.)

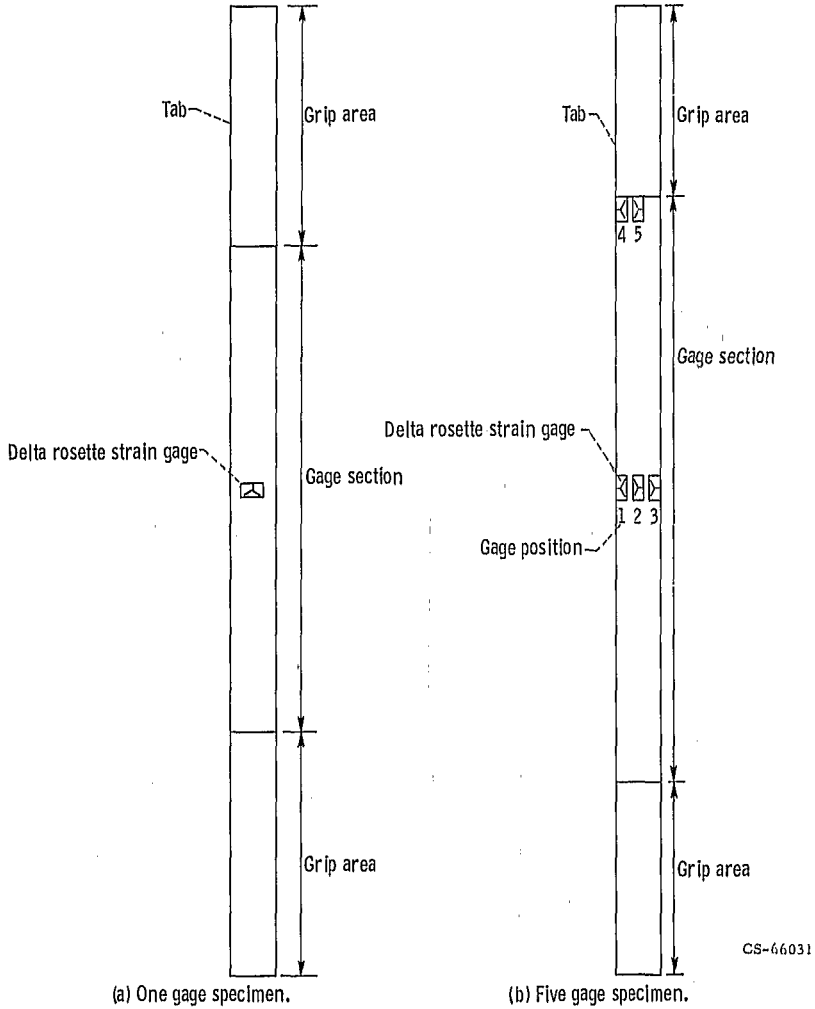

Figure 8. - Schematic of specimen geometry and strain gage arrangement.

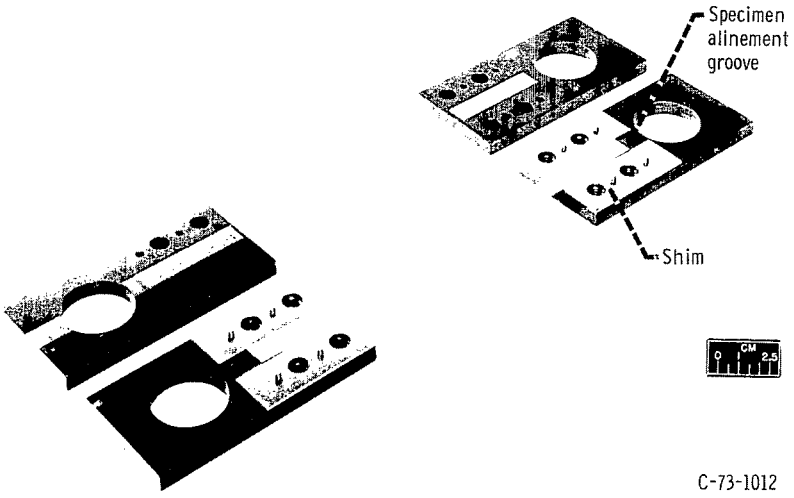

(a) Grips disassembled.

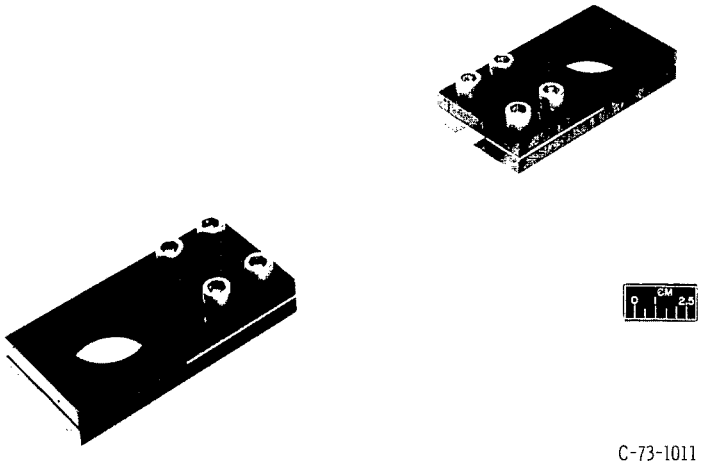

(b) Grips assembled.

Figure 9. - Grips for composite tensile specimens.

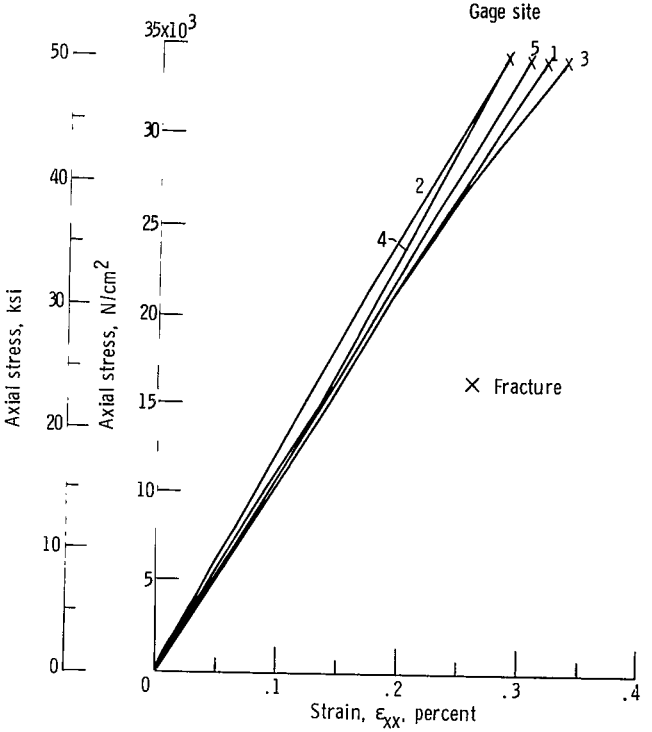

Figure 10. - Stress strain curves at various gage sites (fig. 8) for the 10^0 off-axis tensile specimen (Mod-I/epoxy fiber composite).

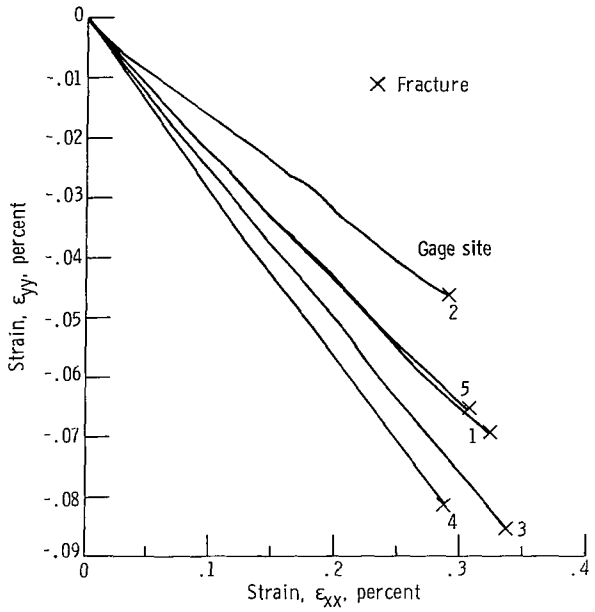

Figure 11. - Transverse (Poisson) strain curves at various gage sites (fig. 8) for 10^0 off-axis tensile specimen (Mod-I/epoxy fiber composite).

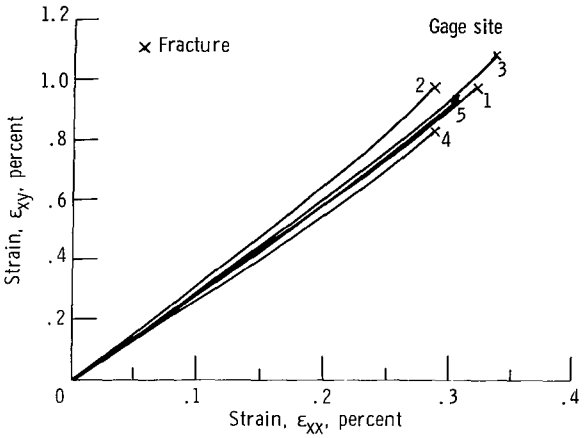

Figure 12. - Shear strain curves at various gage sites (fig. 8) for 10^0 off-axis tensile specimen (Mod-I/epoxy fiber composite).

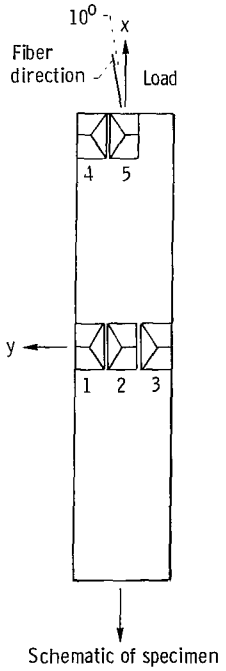

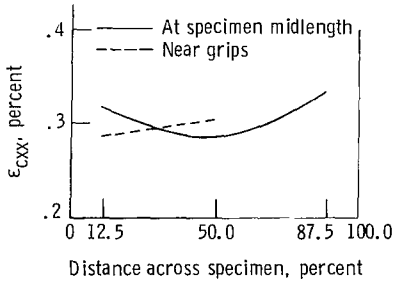

AXIAL STRAINS AT FRACTURE

Gage	Fracture axial strains, percent
1	0.320
2	.287
3	.336
4	.288
5	.305

Figure 13. - Axial strain variation across specimen of Mod-I/epoxy unidirectional composite $[0]_8$ loaded to fracture at 10^0 from fiber direction.

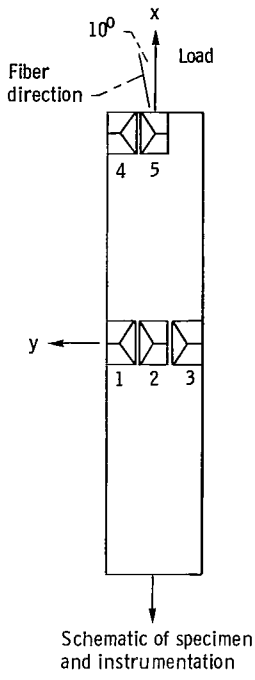

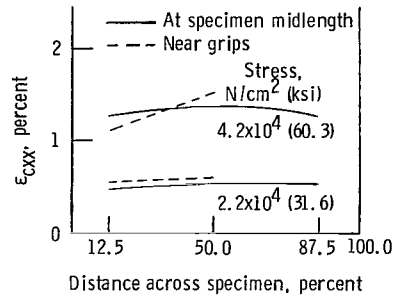

AXIAL STRAINS AT TWO STRESS LEVELS

Gage	Measured strain, percent	
	At fracture	At intermediate stress
1	1.30	0.48
2	1.39	.55
3	1.29	.54
4	1.12	.56
5	1.54	.61

Figure 14. - Axial strain variation measured across specimen of S-glass/epoxy unidirectional composite $[0]_8$ loaded to fracture at 10^0 from fiber direction.

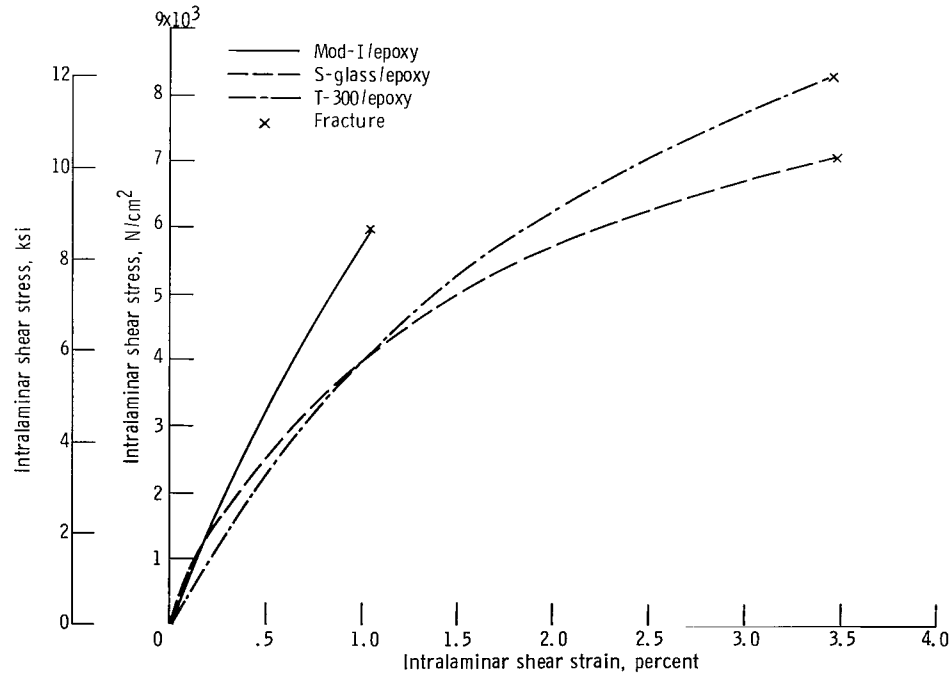

Figure 15. - Intralaminar shear stress-strain diagrams for three materials.

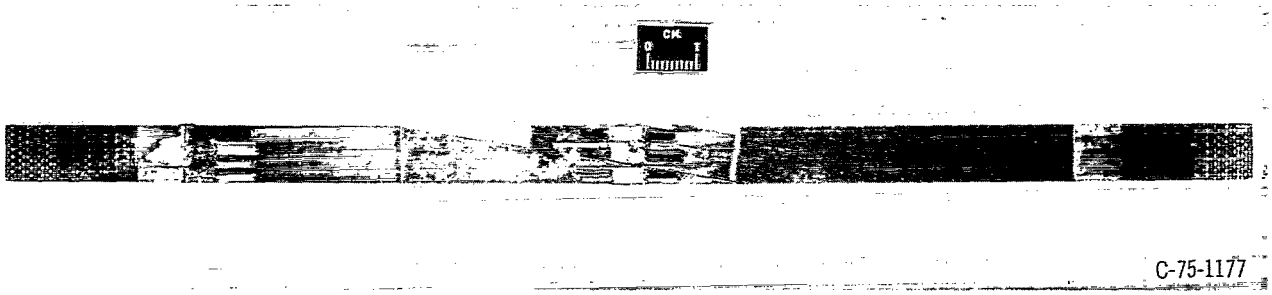

C-75-1177

(a) Front side.

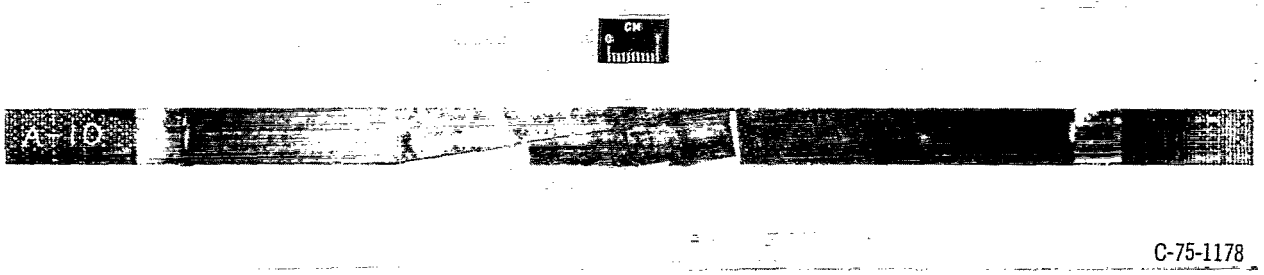

C-75-1178

(b) Back side .

Figure 16. - Photograph of fracture specimen. Mod-I/epoxy.

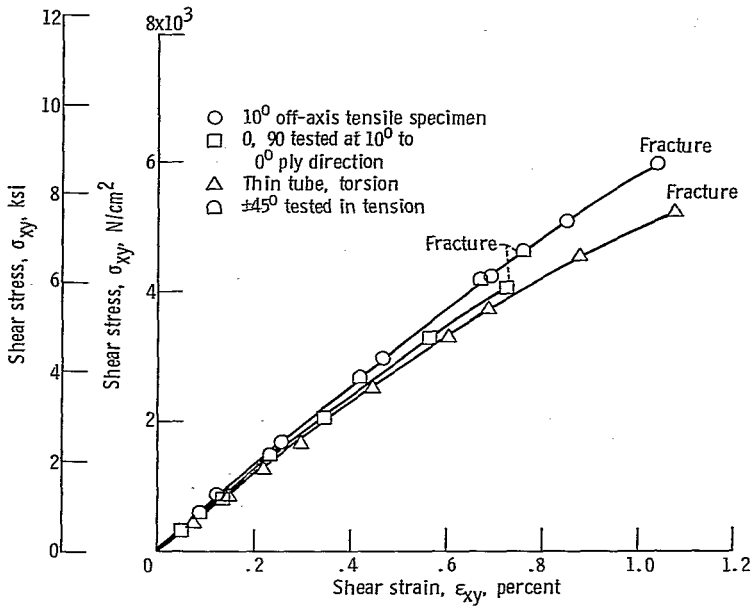

Figure 17. - Comparison of shear stress-strain curves.

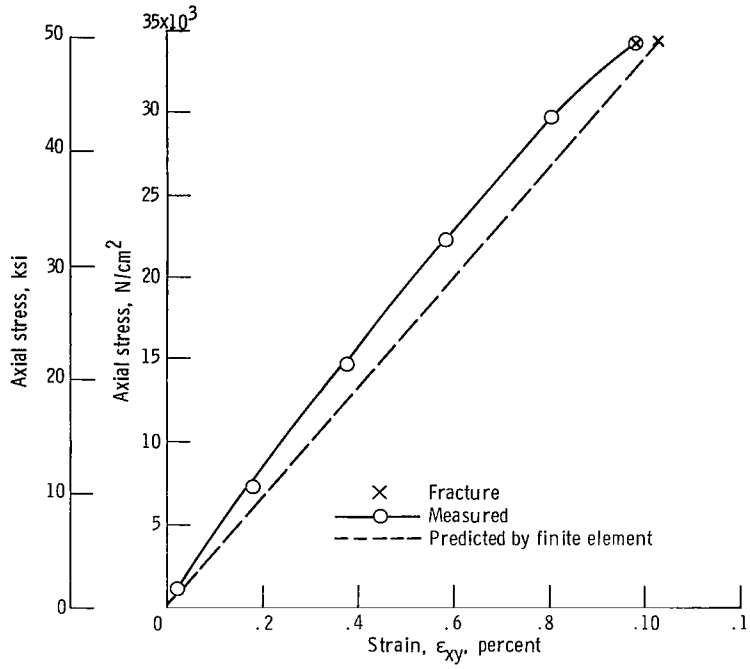

Figure 18. - Comparison of measured and predicted structural axes shear strains strains at center point of 10^0 off-axis tensile specimen (Mod-I/epoxy fiber composite).

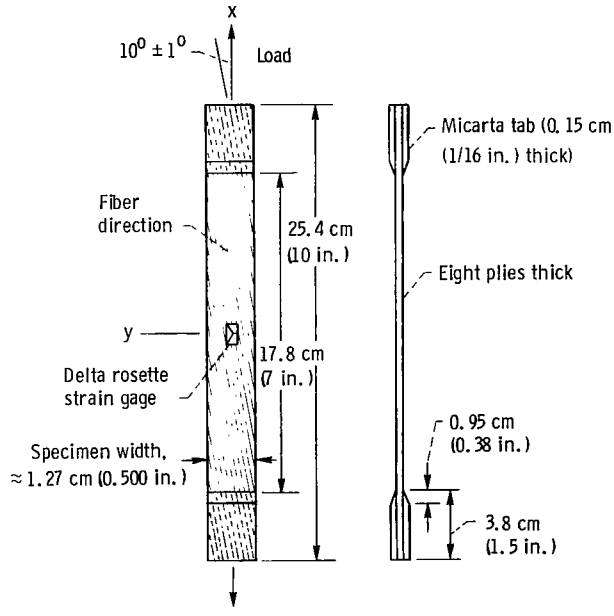

Figure 19. - Schematic showing geometry and instrumentation of proposed 10^0 off-axis tensile specimen for fiber composite intralaminar shear characterization.

"The aeronautical and space activities of the United States shall be conducted so as to contribute . . . to the expansion of human knowledge of phenomena in the atmosphere and space. The Administration shall provide for the widest practicable and appropriate dissemination of information concerning its activities and the results thereof."

—NATIONAL AERONAUTICS AND SPACE ACT OF 1958

NASA SCIENTIFIC AND TECHNICAL PUBLICATIONS

TECHNICAL REPORTS: Scientific and technical information considered important, complete, and a lasting contribution to existing knowledge.

TECHNICAL NOTES: Information less broad in scope but nevertheless of importance as a contribution to existing knowledge.

TECHNICAL MEMORANDUMS: Information receiving limited distribution because of preliminary data, security classification, or other reasons. Also includes conference proceedings with either limited or unlimited distribution.

CONTRACTOR REPORTS: Scientific and technical information generated under a NASA contract or grant and considered an important contribution to existing knowledge.

TECHNICAL TRANSLATIONS: Information published in a foreign language considered to merit NASA distribution in English.

SPECIAL PUBLICATIONS: Information derived from or of value to NASA activities. Publications include final reports of major projects, monographs, data compilations, handbooks, sourcebooks, and special bibliographies.

TECHNOLOGY UTILIZATION PUBLICATIONS: Information on technology used by NASA that may be of particular interest in commercial and other non-aerospace applications. Publications include Tech Briefs, Technology Utilization Reports and Technology Surveys.

Details on the availability of these publications may be obtained from:

SCIENTIFIC AND TECHNICAL INFORMATION OFFICE

NATIONAL AERONAUTICS AND SPACE ADMINISTRATION

Washington, D.C. 20546